Contents lists available at ScienceDirect

Journal of Organometallic Chemistry

journal homepage: http://ees.elsevier.com

Organometallic gold nanoparticles and thin films from cis- and trans-tetrazonium gold(III) salts for electrochemical and photothermal mirror properties

Seema Panicker [a], Aristides Marcano [b], Shehu Isah [c], Brianna Kenney [c], Bizuneh Workie [c], Changseok Han [d,e], Haesung Lee [d], Mohamed M. Chehimi [f], Ahmed A. Mohamed [a,*]

[a] Department of Chemistry, College of Sciences, University of Sharjah, Sharjah 27272, UAE
[b] Division of Physics, Engineering, Mathematics, and Computer Science, Delaware State University, 1200 DuPont HWY, Dover, DE 19901, United States
[c] Department of Chemistry, Delaware State University, 1200 DuPont HWY, Dover, DE 19901, United States
[d] Department of Environmental Engineering, INHA University, Korea 22212
[e] Program in Environmental & Polymer Engineering, Graduate School, INHA University, Korea 22212
[f] Univ Paris Est Creteil, CNRS, ICMPE, UMR7182, F-94320 Thiais, France

ARTICLE INFO

Article history:
Received 13 October 2020
Received in revised form 27 December 2020
Accepted 2 January 2021
Available online xxx

Keywords
Tetrazonium gold
Gold-aryl nanoparticles
Electrochemistry
Thin films
Photothermal mirror

ABSTRACT

Tetrazonium gold(III) salts of syn-(*cis*) and anti-(trans) geometry of 4,4′-(1,3-phenylenediisopropylidene)bisaniline and 4,4′-(1,4-phenylenediisopropylidene)bisaniline were synthesized. $HAuCl_4$ was used as a metal-based counter anion precursor. The gold-carbon nanoparticles (AuNPs) were constructed using the mild reducing agent organoborane 9-borabicyclo[3.3.1]nonane (9-BBN). The nanoparticles dispersed in acetonitrile showed a plasmon peak at 540 nm. Dynamic light scattering measurements showed the size of cis-AuNPs is smaller than the trans-AuNPs. Transmission electron microscopy images showed the formation of spherical shaped AuNPs. X-ray diffraction, energy dispersive spectroscopy, and X-ray photoelectron spectroscopy results supported the presence of metallic gold in both the *cis* and trans AuNPs. Electrochemical studies of the tetrazonium salts showed the facile reduction and the blocking effect of the films formed on glassy carbon electrodes. The photothermal mirror method was used to study the thermal diffusivity of gold thin films deposited over a glassy carbon substrate. The values of the thermal diffusivity coefficient were determined for the *cis* and trans isomers of the film.

1. Introduction

Organometallic gold nanoparticles have raised immense interest over the past two decades because of their widespread applications in *e.g.* nanomedicine [1], catalysis [2], environmental analysis [3], and the energy sector [4]. In particular, aryl-modified gold nanoparticles have proved to be highly stable [5] and could be designed through the spontaneous reaction of aryldiazonium salts with gold nano- and microstructures [6–8], or phase-transfer reactions involving a diazonium salt in organic medium and gold (III) salt in an aqueous solution. The reaction yields AuNPs grafted with aryl monolayer [9]. Alternatively, aryl-capped AuNPs could be prepared using the emergent aryldiazonium tetrachloroaurate(III) salts [10]. These salts are very stable at room temperature and undergo a reductive process that affects both the diazonium and the $[AuCl_4]^-$ anion, which is unique among all kinds of diazonium salts described so far [11]. Such a reduction reaction yields aryl-capped gold nanoparticles for numerous applications in forensic science, catalysis, nanomedicine, and energy [12].

To sum up, in recent years, it became clear that diazonium salts constitute excellent alternatives to the traditional silanes for the modification of metals and other surfaces; and thiols which are employed to modify gold and gold nanoparticles via interfacial Au-S bonds. For this reason, researches also focused on multidiazonium, bisdiazonium, and even tetradiazonium salts. Among them, bisdiazonium salts are efficient surface modifiers for fabricating electrochemically active coating via Gomberg arylation or azo coupling [13]. Bisanilines could be *in situ* diazotized to provide aminobenzene diazonium salts that graft to surfaces and the free amine can, in turn, be diazotized for further reactions. This led to the design of unique micro/nano hierarchical carbon fiber/carbon nanotube reinforcements for polymer matrices [14]. In the case of tetradiazonium salts, Mattiuzi et al. [15] reported grafting calixarenes to gold surfaces using *in situ* generated calix[4]tetradiazonium from tetraaniline precursors. This concept led to the establishment of a new startup in Belgium called X4C [16].

Despite the efficacy of aryldiazonium salts in the reaction with surfaces, it is still important to consider the position of the substituents on the benzene rings and their steric effects. For example, Pinson and co-workers [17] demonstrated that no grafting occurs for an aryldiazonium salt with bis-*tert*-butyl groups at 2- and 6-positions, but a monolayer can be constructed for 3- and 5-positions, while bis-methyl groups at 3- and 5-positions yield oligo aryl layer (termed "multilayer"). The position of the groups presented an important effect

* Corresponding author.
E-mail address: ah.mohamed@sharjah.ac.ae (A.A. Mohamed)

https://doi.org/10.1016/j.jorganchem.2021.121681
0022-328/

on the reactivity of the aryl-modified materials. For example, the team of Strzemiecka [18] demonstrated that the ortho position of the $–CH_2OH$ functional groups sterically hinders grafting the aryl groups to the zeolite filler particles compared to the para position. The phenolic resin filled with aryl-grafted zeolite flows in the case of ortho position whilst the para position yields viscous resin. Interestingly, the cured filled resin exhibited better mechanical properties when $–CH_2OH$ group is in the para position.

There are other types of isomers such as *cis* and trans. Bisdiazonium salts discussed above concerned two diazonium groups borne by the same phenyl rings. If we consider bisdiazonium salts derived from phenylenediisopropylidene bisanilines, diazotization will provide two isomers of the tetrazonium salts: syn (*cis*) and anti (trans) (Fig. 1).

Tetraazotized or bisdiazonium salts are important in surface modification, high-performance adhesives, membrane polymers, copolymerization to construct polyconjugated copolymers with semiconducting properties, wool keratin dying, induce strand session in DNA by forming diradicals, staining red blood cells, and studying cell components [19]. A report claimed the stabilization of tetrazonium salts using zinc(II) chloride counter anion, however, the single-crystal structure was not included [20].

Motivated by previous results showing the direct impact of the molecular structure on macroscopic properties of materials [17,18], we reasoned that *cis* and trans isomers could lead to different reactivities and thus different functionalities of the end arylated materials. Cis- and trans-bisdiazonium isomers have not been investigated in materials modification so far, hence the interest in this study and the promises it holds will expand the knowledge of the colloid and surface science of aryldiazonium salts from a general viewpoint.

In this study, we report a simple and general strategy for the synthesis of AuNPs through the reduction of tetrazonium gold salts which produces aryl covalently functionalized gold nanoparticles. We used the syn (*cis*) and anti (*trans*) isomeric forms of the organic ligand, 4,4′-(1,3-phenylenediisopropylidene)bisaniline and 4,4′-(1,4-phenylenediisopropylidene)bisaniline to form the organic shell modifier. Usually, acyclic *trans* isomers are more stable than *cis* isomers. The organometallic nanoparticles thus formed are believed to be one of the most robust forms of the nanoparticles. To the best of our knowledge, many studies have been conducted regarding different shapes and sizes of nanoparticles [5] but the use of ligands with two different syn (*cis*) and anti (*trans*) isomeric forms has not been reported so far. We describe the first report on the application of bisdiazonium salts derived from phenylenediisopropylidene bisanilines in the construction of covalently functionalized gold nanoparticles.

The chemical and electrochemical reductive processes were conducted in suspensions as well as on glassy carbon electrodes to provide gold-carbon nanoparticles and films, respectively. The electrochemically generated materials were characterized by cyclic voltammetry for their blocking effects and robustness in aqueous media and organic solvents and photothermal mirror (PTM) techniques, the salient features of which will be summarized [28-34].

2. Experimental section

2.1. Chemicals

4,4′-(1,3-Phenylenediisopropylidene)bisaniline (99%) and 4,4′-(1,4-phenylenediisopropylidene)bisaniline (99%), 9-borabicyclo[3.3.1]nonane solution (0.5 M in THF), tetrahydrofuran (Chromasolv Plus, inhibitor-free HPLC grade), ethanol (99.8%), hydrochloric acid (36.5–38%), and acetonitrile (HPLC grade) from Sigma-Aldrich. Sodium nitrite (98%), and sodium sulfate (99%) from Merck Chemicals. $HAuCl_4$ was synthesized in our lab. Sodium chloride (99.5%) from Wardle Chemicals. Deionized (DI) water was used for all lab purposes.

2.2. Synthesis of tetrazonium gold salts

One mmol (0.5 g) of each of the bisaniline ligands was dissolved separately in 100 mL of DI water and 10 mL of 6 M HCl and stirred at high speed to get a clear solution (Solution A). Solutions were kept in an ice bath to maintain the temperature below 5 °C. Three mmol (69 mg) of sodium nitrite was dissolved in DI water and was kept in an ice bath (solution B). Solution B was then added dropwise to solution A in an ice bath and stirred. This resulted in the formation of tetrazonium salts. The formation of tetrazonium salts was confirmed by azo coupling with 2-naphthol/NaOH to give a dark orange color of the diazine. The second step was the chloride counter ion exchange with 1 g (2 mmol) of $HAuCl_4$ acid in DI water. The exchange reaction in water resulted in the formation of tetrazonium tetrachloroaurate(III) salt. The solution was filtered and the yellow precipitate was collected and air-dried for further use in the synthesis of the gold nanoparticles.

2.3. Synthesis of gold nanoparticles

A 0.5 g weight of the cis- and trans-tetrazonium tetrachloroaurate(III) salt was taken in 50 mL of DI water and stirred. The reducing agent 9-BBN of 4 mL was added over 1 h to the above solution under stirring. The color changed from yellow to black, and the solution was stirred for 2 h. The suspended nanoparticles were then allowed to settle and subsequently, the solvent was decanted. The sediments were washed twice in water and then subjected to dialysis for 48 h against water. The suspended nanoparticles in water were centrifuged for 10 min at 3500 rpm and the black deposits of the nanoparticles were collected, washed with DI water, and air-dried.

2.4. Dispersibility tests and phase-transfer of nanoparticles

Dispersibility of the tetrazonium gold salts and the nanoparticles was examined using acetonitrile, water, and tetrahydrofuran (THF). Briefly, 2 mg of the cis- and trans-tetrazonium gold salts and AuNPs were dissolved in 3 mL each of the solvents and stirred vigorously for 20 min. For a typical phase-transfer experiment, 2 mL each of the cis- and trans-AuNPs in aqueous solutions were taken in vials and 2 mL of THF and toluene solutions were added to each vial. The solutions were stirred and allowed to stand for 20 min.

2.5. Characterization

UV–vis absorption spectra were measured using Spectro UV-2510TS in the range of 200–800 nm with 2 nm resolution. FT-IR spectra were recorded on a Bruker (Platinum ATR) Tensor II FT-IR spectrophotometer. Raman spectra of the tetrazonium gold salts were obtained using Renishaw InVia Raman Spectrometer, UK. The laser source used was 514 nm. Oxford Instruments X-Max

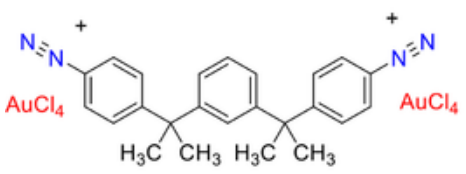

Cis-tetrazonium gold(III) salt

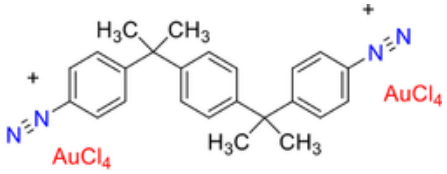

Trans-tetrazonium gold(III) salt

50 EDS detector (LN2 free system) was used. XRD data were obtained by using Bruker D8 Advance with a maximum voltage of 40 kV and a maximum current of 40 mA. The X-ray source was Cu. The size of nanoparticles in solution was obtained using DLS, Microtrac–Nanotrac Wave II (Model MN 42x), containing solid-state diode lasers of wavelength 780 nm. The optical powers of the lasers were 3–5 mW. The temperature was between 10 and 40 °C. XPS analyses of aryl-capped gold particles were conducted using a K Alpha apparatus (Thermo, East-Grinsted, UK) equipped with a monochromatic Al Ka source ($h\nu$ = 1486.6 eV). The samples were mounted on a powder sample holder and analyzed under continuous charge compensation with an electron flood gun. The pass energy was set to 200 eV and 80 eV for recording the survey and narrow regions, respectively.

2.6. Transmission electron microscopy analysis

To investigate the morphology of the samples, a transmission electron microscope (TEM, JEOL JEM-2010F) was used with a field emission gun at 200 kV. For the analysis, two drops of each sample suspended in acetonitrile were immobilized on each Formvar carbon film TEM grid (FCF-400-Cu, Electron Microscopy Science).

2.7. Electrochemistry measurements

Cyclic voltammetry (CV) studies were performed using CH Instrument electrochemical analyzer Model 660 A comprised of a 3 mm diameter glassy carbon (GC), Pt wire counter electrode, and Ag/AgCl, KCl (saturated) reference electrode. GC working electrode was polished with 0.05 μm Buehler micro polish alumina powder, washed with deionized water, sonicated for 5 min, and dried with acetone. A 0.10 mM solution of the cis- and trans-tetrazonium gold salts were used in all experiments with 0.1 M tetrabutylammonium hexafluorophosphate (TBAHFP) supporting electrolyte in acetonitrile (CH_3CN). Before the electrochemical measurements, the solutions were bubbled for 10 min and were blanketed with nitrogen gas while conducting the experiments. Background cyclic voltammograms were acquired before the tetrazonium gold salts addition. Potentials are reported *versus* Ag/AgCl, KCl (saturated) reference electrode at room temperature and are not corrected for liquid junction potentials.

2.8. Photothermal mirror (PTM) method [21]

Fig. 2 shows a simplified scheme of the homemade PTM spectrometer. A 0.2 W CW diode-pumped laser working at 532 nm provides the pump light. A signal generator modulates this light at frequencies from 0.1 to 1000 Hz. A 15-cm focal length lens focuses the pump beam onto the sample. The resulting beam spot diameter is 47 ± 10 μm. A 2 mW He-Ne laser (632 nm) provides the probe beam. The mirror M1 directs this light toward the sample in such a way that the probe beam center coincides with the focused spot of the pump beam. The probe beam spot diameter is 2 mm. Mirror M2 redirects the reflected probe beam toward an interference filter for 632 nm, and to aperture A. The interference filter depletes any residual pump light. Behind this aperture, a diode detector (Det) registers the probe beam transmission. The signal is then amplified using a current preamplifier Apl (ST 540 Stanford Research System) before sending it to a digital oscilloscope Osc for processing. The oscilloscope monitors the time dependence of the probe power transmitted through the aperture as a function of time.

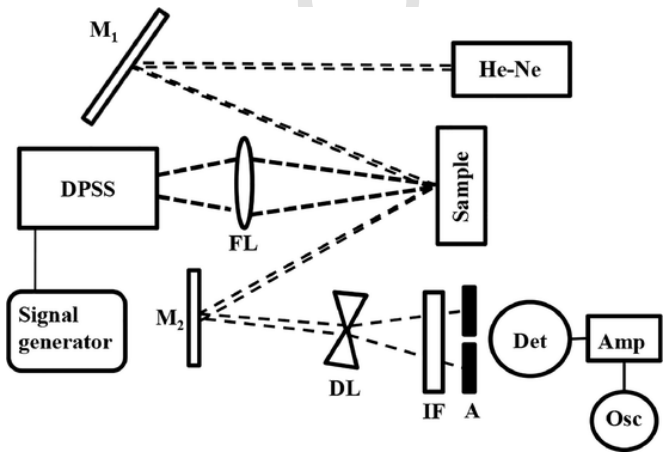

Fig. 2. PTM spectrometer composed of laser pump DPSS, signal generator, laser probe He-Ne, mirrors M1 and M2, focusing lens FL, sample, defocusing lens DL, interference filter, aperture A, semiconductor detector, current preamplifier, and digital oscilloscope.

3. Results and discussions

3.1. Characterization

The tetrazonium gold salts were found to be completely soluble in CH_3CN and THF. The salts in water were subjected to high-speed stirring and sonication to get a suspended solution of tetrazonium gold salts before the addition of the reducing agent. Gold-aryl nanoparticles were synthesized using the mild reducing agent organoborane 9-borabicyclo[3.3.1]nonane (9-BBN). The mild reducing agent 9-borabicyclo[3.3.1]nonane (9-BBN) was used in the construction of phosphine- and thiolate-stabilized AuNPs. The 9-BBN was used in the synthesis of triphenylphosphine-stabilized AuNPs with diameters of 1.2–2.8 nm and narrow size distribution. Also, 9-BBN was used as a mild reducing agent for the synthesis of a series of functionalized alkyl thiolate, bifunctional alkane thiolate [22–24], and arene thiolate-stabilized AuNPs [25].

The phase-transfer behavior of gold nanoparticles synthesized in water was checked in THF and toluene. THF was found to be completely miscible with nanoparticles in water, while in toluene there was no phase-transfer. There was a colorless upper layer of toluene and the lower layer had nanoparticles still in the water. From this study, we concluded that the nanoparticles were dispersible in THF and indispersible in toluene.

The thermal decomposition of cis- and trans-tetrazonium gold salts were investigated. The yellow-colored cis-tetrazonium gold salt decomposed at 98 °C, while the trans-tetrazonium gold salt decomposed at 118 °C. The two salts decomposed to dark brown oil with the evolution of gas due to tetrazonium nitrogen loss. The decomposition temperature of the cis-tetrazonium gold salt matches that of the bisaniline ligand of 98 °C, however, that of the trans isomer decreased from 165–166 °C to 118 °C. In conclusion, trans-tetrazonium is thermally more stable than the cis-tetrazonium gold salt.

The conductance of the tetrazonium gold salts was measured. The solutions of 10 mM NaCl and Na_2SO_4 in water were taken as references. Each of the cis-, trans-, and Br-4-diazonium gold salts solution of 10 mM was dissolved in a mixture of 2 mL of CH_3CN and 3 mL of water. From the results, it can be concluded that the conductance of the cis- and trans-tetrazonium salts, which carries a charge ratio of 1:2 is not the double of the conductance of Br-4-diazonium gold salt, which carries a charge ratio of 1:1. Our results are compared with NaCl which has a charge ratio of 1:1 and Na_2SO_4 which has a charge ratio of 1:2. The conductance is not double as expected, based on their charge distribution. However, the cis-tetrazonium gold salt possesses a slightly higher conductance value than the trans isomer (Table 1).

UV–vis spectroscopy is extensively used in nanotechnology as an analytical tool to confirm the formation of nanoparticles and their dispersibility. The spectroscopic properties of nanoparticles provide detailed information about

Table 1
Conductance measurements in water.

Salt Solution	Conductance (S/cm)
NaCl	2.92
Na_2SO_4	5.68
Cis-tetrazonium gold salt	0.314
Trans-tetrazonium gold salt	0.249

their size distribution based on the position of the surface plasmon peak [26]. The cis-AuNPs in acetonitrile (Fig. 3A) shows a peak at around 550 nm, corresponding to the plasmon excitation, while the plasmon peak for the trans-AuNPs (Fig. 3A) is red-shifted to 600 nm. UV–vis results of the AuNPs in different solvents showed both cis- and trans-AuNPs increased in size in THF, as the UV–vis peak was seen to be redshifted towards the range of 600–700 nm. This was further supported by size distribution results from DLS which showed a very high range of sizes for the cis- and trans-AuNPs in THF. Overall results showed that the cis-AuNPs are smaller in size than the trans-ANPs isomer (Fig. 3B).

FT-IR spectra of the cis- and trans-bisaniline ligands 4,4′-(1,3-phenylenediisopropylidene)bisaniline (*cis*) and 4,4′-(1,4-phenylenediisopropylidene)bisaniline (trans) display two bands assigned to NH_2 functional groups centered at 3400 cm^{-1}. The presence of C—H bonds can be confirmed from the bands at 2900 cm^{-1}. Raman spectra of both the cis- and trans-tetrazonium gold salts were obtained using a laser source of 514 nm. Two sharp peaks assigned for $[AuCl_4]^-$ due to Au-Cl stretching frequency were obtained at approximately 344 and 337 cm^{-1} and the tetrazonium peak at 2264 cm^{-1}. IR spectra of cis- and trans-tetrazonium gold salts suggest the presence of tetrazonium at 2263 cm^{-1}. IR spectra of the gold nanoparticles showed the absence of the diazonium stretch. The presence of the phenyl ring can be observed at the same position for the bisaniline ligands. The peak of the phenyl ring for the $C = C$ bond can be observed at 1600 and 1400 cm^{-1} which confirms the presence of the organic shell connected to the gold core.

3.2. EDS and XRD analysis

EDS results from two different sites of the cis-AuNPs showed 16.8–22.6% gold and 67.8–73% carbon. Results from two different sites of the trans-AuNPs showed 32.1–35.5% gold and 54.5–56.2% carbon. XRD analysis of the gold nanoparticles is represented by five peaks corresponding to Bragg reflections (111), (200), (220), (311), and (222) of the face-centered cubic lattice. The intense peak at $2\Theta = 38.1^{\circ}$ represents preferential growth in the (111) direction.

3.3. TEM analysis

The formation of AuNPs was investigated using TEM. As seen in Fig. 4, most AuNPs for both *cis* and trans are spherical, especially for the *cis* sample.

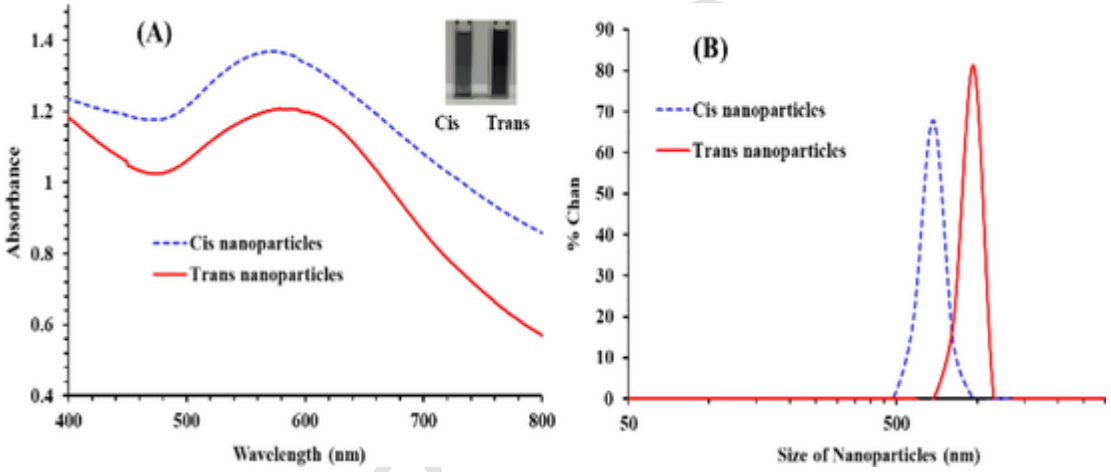

Fig. 3. (A) UV–vis of cis- and trans-AuNPs in acetonitrile and (B) DLS size measurement of cis- and trans-AuNPs in acetonitrile.

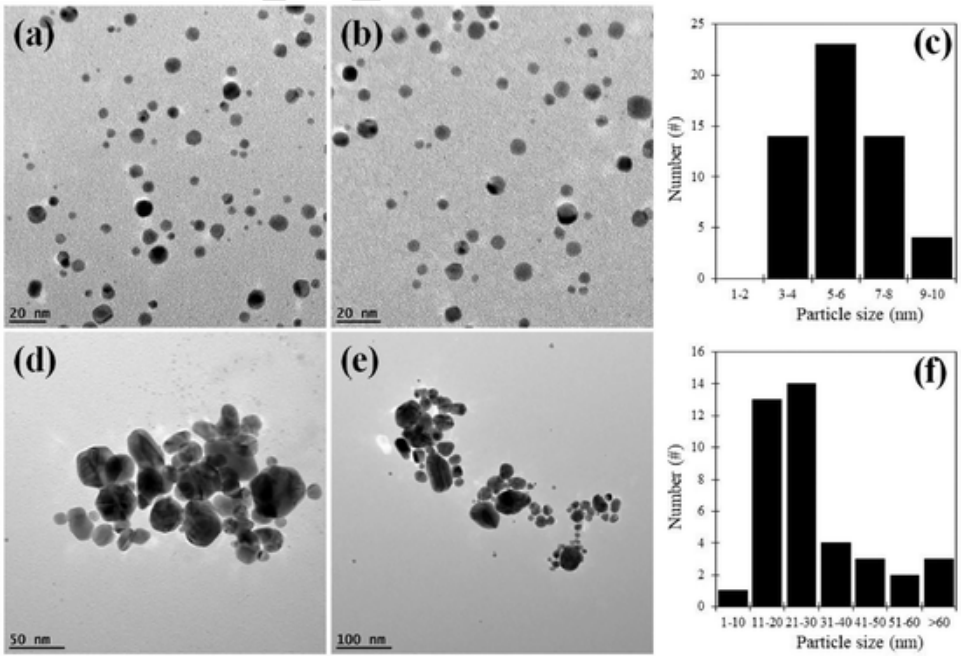

Fig. 4. (a) & (b) TEM images of cis-AuNPs, (c) cis-AuNPs particle size distribution, (d) & (e) TEM images of trans-AuNPs, and (f) trans-AuNPs particle size distribution.

For trans samples, oval and triangular AuNPs were observed. The clear difference between *cis* and trans samples was the size distribution of AuNPs. For the *cis* sample, very uniform spherical AuNPs with an average size of 6.1 ± 1.7 nm were synthesized and ranged from 3.1 to 9.9 nm, however, for the trans sample, particle sizes ranged from 9.8 to 73.8 nm and the average size was 28.6 ± 16.9 nm. It clearly showed much larger AuNPs produced in the case of the trans sample compared to cis-AuNPs, and it is in good agreement with DLS analysis. Trans sample might form interconnected networks which leads to aggregation.

3.4. XPS analysis

XPS was used to supplement the EDS results to check whether the surface of the particles is representative of the bulk or if any depletion occurs for one of the elemental markers of the core and the shell. Fig. 5 displays Au4f, N1s, and C1s peaks from the cis- and trans-AuNPs. The *cis* nanoparticles exhibit noisy Au4f doublet (Fig. 5a) compared to the trans-AuNPs (Fig. 5b), with $Au4f_{7/2}$ centered at 84 eV, in line with the metallic character of the core. N1s spectra from cis- and trans-AuNPs are shown in Figs. 5c and d, respectively. This shows that the reduction of the tetrazonium leads to AuNPs with possible azo linkages within the capped aryl layer. Although N1s spectra are noisy due to the low extent of nitrogen, one can note distinct fine structures recorded for cis- and trans-AuNPs. The main peak components are centered at 400 eV and could be assigned to $N = N$ linkages. However, one can also note, particularly for cis-AuNPs, a second component that could be assigned to quaternized nitrogen atoms therefore suggesting the existence of protonated azo linkages. This is supported by the existence of Cl2p peaks for both nanoparticles (spectra are not shown).

Fig. 5e displays the C1s peak from trans-AuNPs; the inset shows a zoomed-in region around 291 eV. It testifies to the aromatic nature of the shell. The main peak is almost featureless, with a very light shoulder at a high binding energy side (~286–287 eV) due to C—$N = N$ and possibly some oxidized carbon atoms (C—O).

From the peak area, one could sort the surface C/Au atomic ratio: 541 for cis-AuNPs, and 256 for the trans-AuNPs. These ratios are much higher than those determined by EDS: 49 for cis-AuNPs and 29 for trans-AuNPs. With both C/Au atomic ratios higher in XPS (surface sensitive) analysis compared to EDS (bulk sensitive), XPS results support the core/shell structure of aryl-capped AuNPs.

3.5. Electrochemical studies

Grafting on various surfaces has been utilized in the formation of robust films for applications related to organometallic conducting films. The grafted film from diazonium gold salts has shown outstanding robustness because of the efficient electrochemical grafting [12]. Electrochemical studies were carried out to probe the reducibility of the tetrazonium salts.

The highly irreversible reduction peaks of 0.1 mM cis- and trans-tetrazonium gold salts occurred at −0.030 V and −0.037 V in 0.1 M TBAHFP/acetonitrile *vs* Ag/AgCl, KCl (saturated) at a glassy carbon (GC) working electrode, respectively, Fig. 6. The obtained reduction potential values are close to those of the diazonium gold salts.

Cyclic voltammograms in Fig. 7A show the first cycle overlaid with the second through the tenth cycles for *cis* salt. Figs. 7A exhibits a decrease in the reduction current with an increase in the cycle number, and at the tenth cycle, there is almost no reduction current detected illustrating that the grafting is completed. CV of the reversible redox couple in $[Fe(CN)_6]^{3-/4-}$ was used to study the blocking properties of the grafted film from the cis-tetrazonium gold salt after deposition from ten consecutive cycles in the potential range from +0.50 to −0.80 V *vs.* Ag/AgCl, KCl (saturated). The disappearance of the redox peaks of $[Fe(CN)_6]^{3-/4-}$, Fig. 7B, shows an effective grafting occurred from the cis-tetrazonium gold salt blocking the electron transfer of the $[Fe(CN)_6]^{3-/4-}$. To study the robustness of the grafted films, CV experiments of the reversible redox couples $[Fe(CN)_6]^{3-/4-}$ before and after 1 h sonication of the grafted film from the cis-tetrazonium salt in water, acetonitrile, and toluene were conducted. CV results, Fig. 7C, illustrate the disappearance of the redox

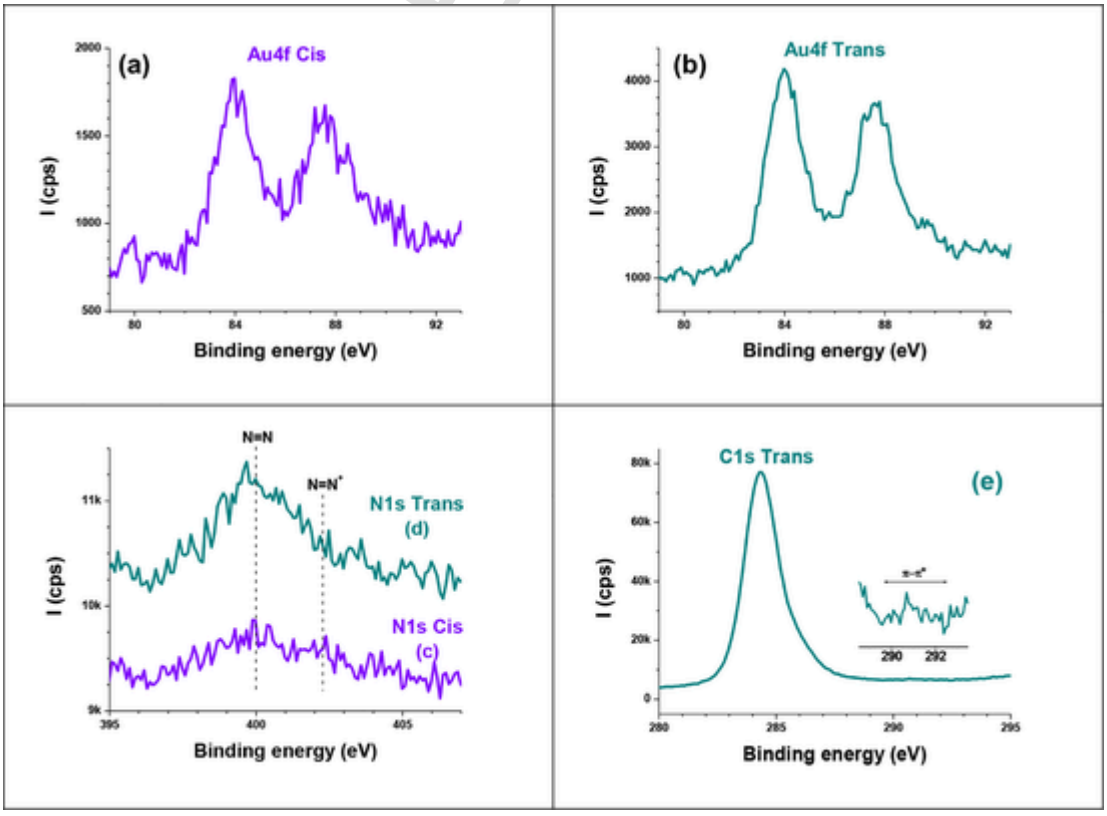

Fig. 5. High resolution XPS spectra Au4f (a-b), N1s (c-d), and C1s (e). For cis-AuNPs: (a) and (c) and for trans-AuNPs: (b), (d), and (e).

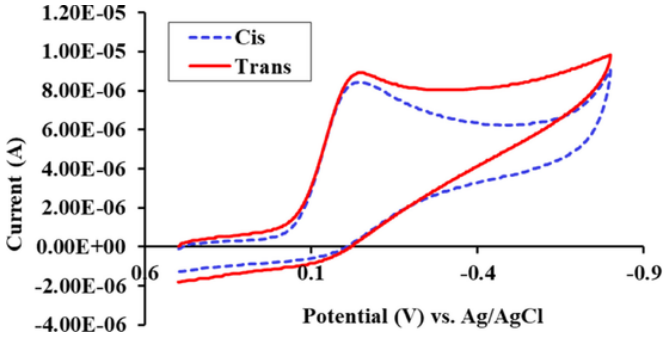

Fig. 6. Overlay of 0.1 mM cis- and trans-tetrazonium gold salts at GC electrode in 0.1 M TBAHFP/acetonitrile at 100 mV/s scan rate.

peaks of $[Fe(CN)_6]^{3-/4-}$ for the grafted film of the cis-tetrazonium salt in water illustrating the robustness of the films.

Similar to the cis-tetrazonium salt, multi-cyclic voltammetric studies of 0.1 mM of trans-tetrazonium gold salt at GC electrode in 0.1 M TBAHFP/acetonitrile at 100 mV/s scan rate from 1st to 10th cycle showed there was almost no reduction current in the 10th cycle illustrating that grafting is completed, Fig. 8A. The reversible redox couple $[Fe(CN)_6]^{3-/4-}$ was used to study the blocking efficiency of trans-tetrazonium film. Fig. 8B illustrates a noticeable reduction peak in $[Fe(CN)_6]^{3-/4-}$, indicating that the blocking of the grafted film is not as efficient as the cis-tetrazonium salt. For the trans-tetrazonium salt, studies to check the robustness of the grafted film exhibit the appearance of noticeable reversible redox peaks of $[Fe(CN)_6]^{3-/4-}$ after sonication in water, acetonitrile, and toluene solvents, Fig. 8C. This demonstrates the grafted film from trans isomer is not as robust as the cis-tetrazonium salt in water. This difference could be due to the porous nature of the trans film due to interlinking networks.

3.6. Photothermal mirror (PTM) method study

We developed a PTM method for the determination of thermal diffusivity of thin films deposited over GC substrates. In the method, a lens focuses an excitation laser beam onto the sample surface generating a thermoelastic deformation of nanometric dimensions or PTM. A second probe beam tests the produced PTM. The reflected probe light exhibits diffraction pattern deformation at the far-field due to the presence of the generated local mirror. A signal was generated by the detection of the probe light transmission through a small aperture. The time evolution of this signal measures the time evolution of the PTM allowing the determination of the sample thermal diffusivity properties. Upon continuous-wave excitation (CW), the PTM signal grows fast during the first microseconds. Later, the signal approaches a stationary value which represents the equilibrium between the intake of heat due to the absorption of light photons by the first atomic layers of the surface and the removal of the heat due to thermal diffusivity. The time evolution is regulated by the PTM time build-up (t_c) which is inversely proportional to the thermal diffusivity coefficient.

A simultaneous resolution of the photo-elastic deformation and the thermal diffusivity equations provides the theoretical background for understanding the properties of the PTM signal, including its time evolution [27–34]. Based on this model, we calculated a universal curve of the signal time evolution expressed in unit-less magnitudes which can be applied in a variety of materials. The curve represents the value of the signal divided over its stationary value as a function of the time divided over the magnitude of the thermal build-up time. We recently used this curve to calibrate a homemade PTM spectrometer and used the calibration to determine the thermal diffusivity coefficients of the films.

The time evolution of PTM signal of the GC substrate was recorded in the absence of films, and GC with *cis* and trans films. The signal was normalized over its stationary value. Then, the experimental results were recorded with the universal PTM signal to obtain the values for the build-up time. The build-up time t_c can be expressed as

$$t_c = \frac{a^2}{4D},$$

where a is the radius of the pump beam spot and D is the thermal diffusivity coefficient.

Fig. 9 shows the normalized PTM signals from the bare GC substrate, and with the *cis* and trans films. The solid red curve corresponds to the universal time behavior curve for the PTM signal calculated using the results of the model published elsewhere [34]. The results showed that the differences are not significant, indicating the synthesized samples are very thermally stable.

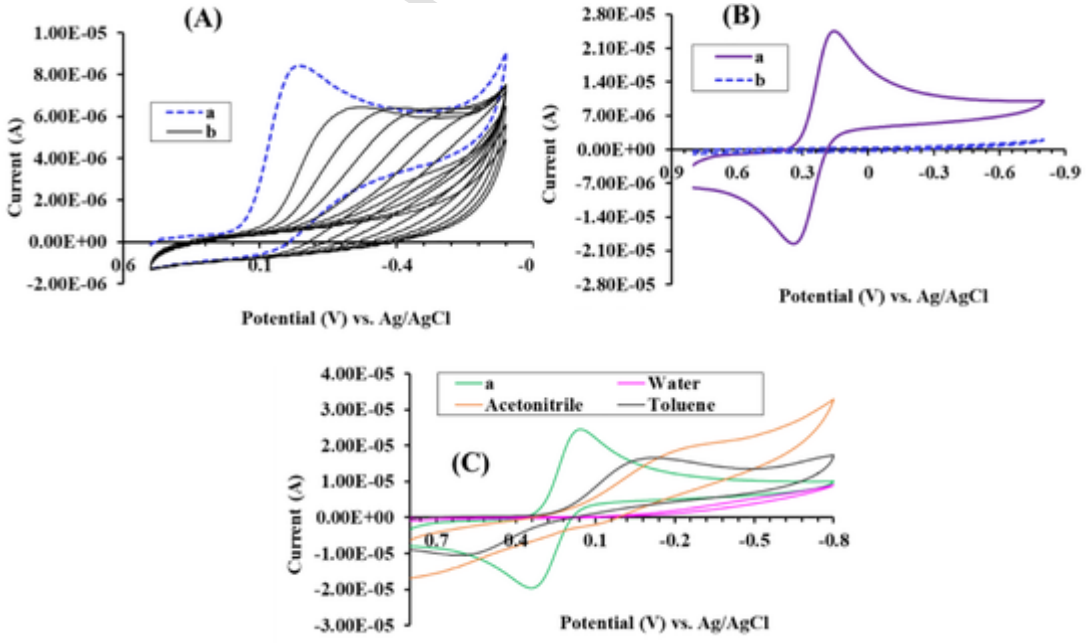

Fig. 7. (A) Cyclic voltammograms of 0.1 mM of cis-tetrazonium gold salt at GC electrode in 0.1 M TBAHFP in acetonitrile at 100 mV/s scan rate (a) 1st run, (b) 2nd to 10th run, (B) Cyclic voltammogram of (a) bare and (b) grafted film from 0.1 mM cis-tetrazonium gold salt at GC electrode in 2.0 mM $K_3[Fe(CN)_6]$ in 1.0 M KNO_3 aqueous solution at 100 mV/s scan rate, and (C) Cyclic voltammogram of 2.0 mM $K_3[Fe(CN)_6]$ in 1.0 M KNO_3 at (a) bare GC electrode and GC electrode modified with cis-tetrazonium gold-carbon film after sonication for 1 h in different solvents.

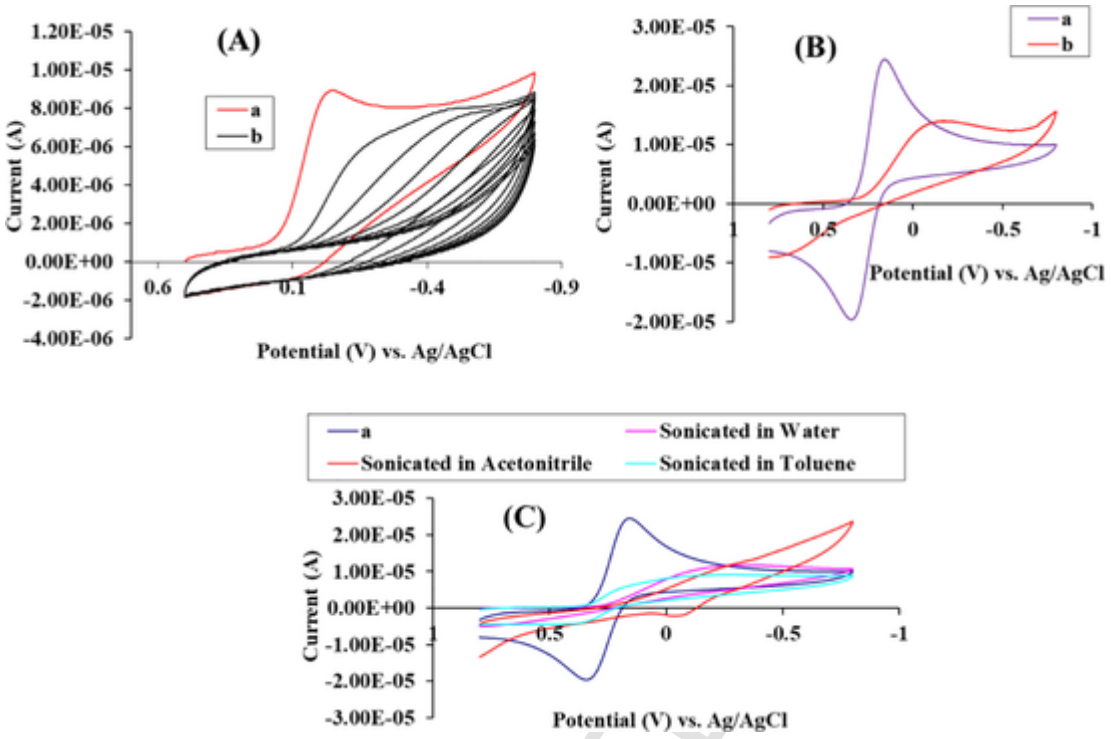

Fig. 8. (A) Cyclic voltammograms of 0.1 mM of trans-tetrazonium gold salt at GC electrode in 0.1 M TBAHFP/acetonitrile at 100 mV/s scan rate (a) 1st run, (b) 2nd to 10th run, (B) Cyclic voltammogram of (a) bare and (b) grafted film from 0.1 mM trans-tetrazonium gold salt at GC electrode in 2.0 mM $K_3[Fe(CN)_6]$ in 1.0 M KNO_3 aqueous solution at 100 mV/s scan rate, and (C) Cyclic voltammogram of 2.0 mM $K_3[Fe(CN)_6]$ in 1.0 M KNO_3 at (a) bare GC electrode and GC electrode modified with trans gold-carbon film after sonication for 1 h in different solvents.

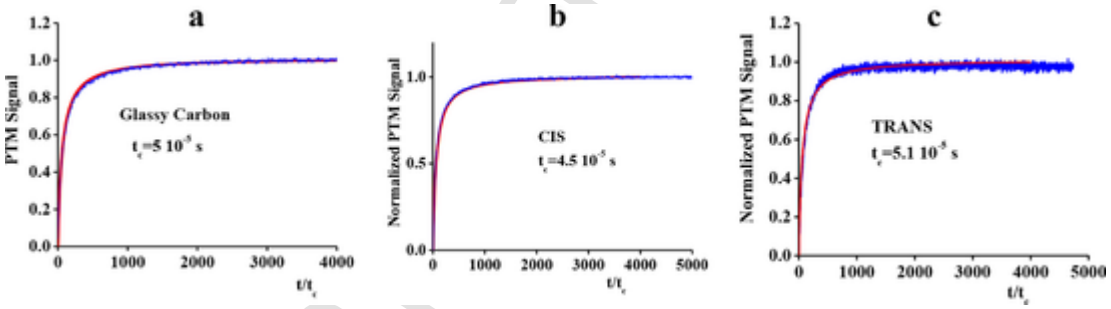

Fig. 9. Normalized PTM signal for the glassy carbon substrate (a) and the glassy carbon with *cis* (b) and trans (c) films.

We have previously estimated the uncoated glassy carbon with a thermal diffusivity of 0.082 $cm^2\ s^{-1}$ [21,34]. Using the measured values of the time t_c, Fig. 9, we estimate for the *cis* sample $D_{cis} = 0.091\ cm^2.s^{-1}$ and for the trans $D_{trans} = 0.080\ cm^2.s^{-1}$. The observed small difference shows that the coating of these samples does not significantly affect the thermal diffusivity properties. The limited coating effect is probably because the absorption of the light photons occurs mostly in bulk.

4. Conclusions

We synthesized two forms of gold nanoparticles using bisaniline ligands with different geometric isomers-syn (*cis*) and anti (trans). The tetrazonium gold salts of both *cis* and trans isomers showed the presence of the tetrachloroaurate(III) bands and the presence of other functional groups, thus confirming the synthesis of tetrazonium gold salts with different geometries. Conductance measurements showed the precursors ionic form to be close to double ionic salts. The gold nanoparticles formed after the tetrazonium gold reduction using a mild reducing agent also showed all their characteristic properties. The electrochemical study proved that the reduction of the salts deposited robust and blocking films on GC substrates.

Declaration of Competing Interest

The authors declare that they have no known competing financial interests or personal relationships that could have appeared to influence the work reported in this paper.

Acknowledgments

AAM acknowledges the University of Sharjah support of SEED grant (VC-GRC-SR-83–2015), competitive grants (160–2142–029-P and 150–2142–017-P), Organometallic Research Group grant (RISE-046–2016), and Functionalized Nanomaterials Synthesis Lab grant (151–0039). BW acknowledges Delaware State University Institute for Science and Technology.

References

[1] E.C. Dreaden, A.M. Alkilany, X. Huang, C.J. Murphy, M.A. El-Sayed, The golden age: gold nanoparticles for biomedicine, Chem. Soc. Rev. 41 (2012) 2740–2779.
[2] M.A. Ortuño, N. López, Reaction mechanisms at the homogeneous–heterogeneous frontier: insights from first-principles studies on ligand-decorated metal nanoparticles, Catal. Sci. Technol. 9 (2019) 5173–5185.
[3] K. Kołątaj, J. Krajczewski, A. Kudelski, Plasmonic nanoparticles for environmental analysis, Environ. Chem. Lett. 18 (2020) 529–542.

[4] X. Yang, Q. Xu, Gold-containing metal nanoparticles for catalytic hydrogen generation from liquid chemical hydrides, Chinese J. Cat. 37 (2016) 1594–1599.
[5] A.A. Mohamed, S.N. Neal, B. Atallah, N.D. AlBab, H.A. Alawadhi, Y. Pajouhafsar, H.E. Abdou, B. Workie, E. Sahle-Demessie, C. Han, M. Monge, J.M. Lopez-de-Luzuriaga, J.H. Reibenspies, M.M. Chehimi, Synthesis of gold organometallics at the nanoscale, J. Organomet. Chem. 877 (2018) 1–11.
[6] L. Laurentius, S.R. Stoyanov, S. Gusarov, A. Kovalenko, R. Du, G.P. Lopinski, M.T. McDermott, Diazonium-derived aryl films on gold nanoparticles: evidence for a carbon gold covalent bond, ACS Nano 5 (2011) 4219–4227.
[7] R. Ahmad, N. Felidj, L. Boubekeur-Lecaque, S. Lau-Truong, S. Gam-Derouich, P. Decorse, A. Lamouri, C. Mangeney, Water-soluble plasmonic nanosensors with synthetic receptors for label-free detection of folic acid, Chem. Commun. 51 (2015) 9678–9681.
[8] O. Guselnikova, V. Svorcik, O. Lyutakov, M.M. Chehimi, P.S. Postnikov, Preparation of selective and reproducible SERS sensors of Hg^{2+} ions via a sunlight-induced thiol–yne reaction on gold gratings, Sensors 19 (2019) 2110.
[9] F. Mirkhalaf, D.J. Schiffrin, Electrocatalytic oxygen reduction on functionalized gold nanoparticles incorporated in a hydrophobic environment, Langmuir 26 (2010) 14995–15001.
[10] S.N. Neal, S.A. Orefuwa, A.T. Overton, R.J. Staples, A.A. Mohamed, Synthesis of diazonium tetrachloroaurate(III) precursors for surface grafting, Inorganics 1 (2013) 70–84.
[11] See section 4.1/Table 3 of the paper A. Bensghaïer, F. Mousli, A. Lamouri, P.S. Postnikov, M.M. Chehimi, The molecular and macromolecular level of carbon nanotube modification via diazonium chemistry: emphasis on the 2010s years, Chem. Africa (2020).
[12] A.A.L. Ahmad, B. Workie, A.A. Mohamed, Diazonium gold salts as novel surface modifiers: what have we learned so far?, Surfaces 3 (2020) 182–196.
[13] N. Marshall, J. Locklin, Reductive electrografting of benzene (p-bisdiazonium hexafluorophosphate): a simple and effective protocol for creating diazonium-functionalized thin films, Langmuir 27 (2011) 13367–13373.
[14] Y. Wang, L. Meng, L. Fan, G. Wu, L. Ma, Y. Huang, Preparation and properties of carbon nanotube/carbon fiber hybrid reinforcement by a two-step aryl diazonium reaction, RSC Adv 5 (2015) 44492–44498.
[15] I.Jabin Mattiuzzi, C. Mangeney, C. Roux, O. Reinaud, L. Santos, J.F. Bergamini, P. Hapiot, C. Lagrost, Electrografting of calix[4]arenediazonium salts to form versatile robust platforms for spatially controlled surface functionalization, Nat. Commun. 3 (2012) 1130.
[16] http://x4c.eu/, last accessed 29 September 2020.
[17] D.-e.Jiang Combellas, F. Kanoufi, J. Pinson, F.I. Podvorica, Steric effects in the reaction of aryl radicals on surfaces, Langmuir 25 (1) (2009) 286–293.
[18] M. Sandomierski, B. Strzemiecka, J. Grams, M.M. Chehimi, A. Voelkel, Diazonium-modified zeolite fillers. effect of diazonium substituent position on the filler surface modification and the mechanical properties of phenolic/zeolite composites, Int. J. Adhes. Adhes. 85 (2018) 157–164.
[19] Y. Sun, Y. Xia, Shape-controlled synthesis of gold and silver nanoparticles, Science 298 (2002) 2176–2179.
[20] S.Siggia Savitsky, Pyrolysis gas chromatography of diazonium salts, Anal. Chem 46 (1974) 149–152.
[21] G.Gwanmesia Marcano, M. King, D. Caballero, Determination of thermal diffusivity of opaque materials using the photothermal mirror method, Opt. Eng. 53 (2014) 127101.
[22] A.I.T. Aybuke, K. Emine, U. Zafer, E. Haslet, O.S. Ali, Z. Betul, Syntheses and modifications of bisdiazonium salts of 3,8-benzo[*c*]cinnoline and 3,8-benzo[*c*]cinnoline 5-oxide onto glassy carbon electrode and the characterization of the modified surfaces, J. Solid-State Electrochem. 16 (2012) 235–245.
[23] G. Chen, M. Takezawa, N. Kawazoe, T. Tateishi, Preparation of cationic gold nanoparticles for gene delivery, Open Biotechnol. J. 2 (2008) 152.
[24] A.J. Di-Pasqua, R.E. Mishler, Y.L. Ship, J.C. Davrowiak, T. Asefa, Preparation of antibody-conjugated gold nanoparticles, Mater. Lett. 63 (2009) 1876.
[25] A.F.G. Leontowich, C.F. Calver, M. Dasog, R.W.J. Scott, Surface properties of water-soluble glycine-cysteamine-protected gold clusters, Langmuir 26 (2010) 1285–1290.
[26] R. Sardar, J.S. Shumaker-Parry, 9-BBN Induced synthesis of nearly monodisperse ω-functionalized alkylthiol stabilized gold nanoparticles, Chem. Mater. 21 (2009) 1167–1169.
[27] T. Elperin, G. Rudin, Thermal mirror method for measuring physical properties of multilayered coatings, Int. J. Thermoph. 28 (2007) 60–82.
[28] N.G.C. Astrath, L.C. Malacarne, P.R.B. Pedreira, A.C. Bento, M.L. Baesso, J. Shen, Time-resolved thermal mirror for nanoscale surface displacement detection in low absorbing solids, Appl. Phys. Lett. 91 (2007) 191908.
[29] F. Sato, L.C. Malacarne, P.R.B. Pedreira, M.P. Belancon, R.S. Mendes, M.L. Baesso, N.G.C. Astrath, J. Shen, Time-resolved thermal mirror method: a theoretical study, J. Appl. Phys. 104 (2008) 053520.
[30] N.G.C. Astrath, L.C. Malacarne, V.S. Zanuto, M.P. Belancon, R.S. Mendes, M.L. Baesso, C. Jacinto, Finite-size effect on the surface deformation thermal mirror method, J. Opt. Soc. Am. B 28 (2011) 1735–1739.
[31] L.C. Malacarne, N.G.C. Astrath, G.V.B. Lukasievicz, E.K. Lenzi, M.L. Baesso, S.E. Bialkowski, Time-resolved thermal lens and thermal mirror spectroscopy with sample-fluid heat coupling: a complete model for material characterization, Appl. Spect. 65 (2011) 99–104.
[32] G.V.B. Lukasievicz, L.C. Malacarne, N.G.C. Astrath, V.S. Zanuto, L.S. Herculano, S.E. Bialkowski, A theoretical and experimental study of time-resolved thermal mirror with non-absorbing heat coupling fluids, Appl. Spect. 66 (2012) 1461–1467.
[33] O.S. Aretegui, P.Y.N. Poma, L.S. Herculano, G.V.B. Lukasievicz, F.B. Guimaraes, L.C. Malacarne, M.L. Baesso, S.E. Bialkowski, N.G.C. Astrath, Combined photothermal lens and photothermal mirror characterization of polymers, Appl. Spectrosc. 68 (2014) 777–783.
[34] G.Gwanmesia Marcano, B. Workie, Photothermal mirror method for the study of thermal diffusivity and thermo-elastic properties of opaque solid materials, Inter. J. Thermoph. 38 (2017) 136.